JOURNAL OF GEOPHYSICAL RESEARCH, VOL. 104, NO. A11, PAGES 25,127-25,141, NOVEMBER 1, 1999

Microstructure of Jovian decametric S bursts

Thomas D. Carr and Francisco Reyes

Department of Astronomy, University of Florida, Gainesville

Abstract. We have developed a method for displaying the spectral structure of Jupiter's decametric radio S bursts on timescales down to a few microseconds, 2 orders of magnitude finer than has been achieved elsewhere. By employing an extremely sensitive antenna (640 dipoles, at 26 MHz) and selecting only relatively weak S bursts that possess the simplest possible spectral shape, we identify frequently occurring structural features that we associate with localized emission centers. On timescales having better than about 30 μs resolution we find that the S burst baseband oscillation (and therefore the RF oscillation) is modulated to form distinct pulses, which we refer to as subpulses. Still finer time resolution reveals that within individual subpulses the baseband (and RF) oscillation often displays segments in which the usually drifting phase term abruptly becomes essentially constant and, after remaining so for 10 to 100 μs, abruptly resumes its random drift. It is these abruptly starting and ending segments of phase coherence that we attribute to isolated powerful centers of cyclotron maser wave amplification, which happen for brief intervals to be the only ones that are active. We believe that the more usual phase-incoherent condition (i.e., one in which the instantaneous frequency drifts randomly within the emission band) is due to the fact that the resultant radiation is the sum of two or more components from neighboring wave amplification centers emitting at slightly different frequencies, with independently varying intensities. Possible models for the production of subpulses and phase coherent intervals are discussed.

1. Introduction

The highly sporadic low–frequency radio emissions from Jupiter's magnetosphere extend from about 10 kHz to 40 MHz. The lower limit is set by the loss of radio transparency of the interplanetary medium. The upper limit, which is relatively sharp [*Warwick*, 1967], is closely related to the fact that it is near the maximum value of the electron cyclotron frequency within the magnetosphere of the planet. The probability of occurrence is at a maximum in the vicinity of 5 or 10 MHz. This radiation has arbitrarily been divided into the kilometer-, hectometer-, and decameter-wavelength components. Only the decametric component is observable from Earth. Most of the terrestrial observations of this component have been made between the frequencies 15 and 27 MHz, because of the increasingly deleterious effects of the terrestrial ionosphere below 15 MHz and the very low occurrence probability of the radiation above 27 MHz. The decametric radiation usually occurs in the form of well-defined noise storms, consisting mainly of the so-called L bursts. The dynamic spectrum (i.e., the plot of intensity versus time and frequency) of a typical L burst consists of Gaussian noise, band-limited to about 3 MHz, which builds up to maximum intensity and decreases to zero within an interval of 2 to 10 s. Intrinsic frequency drifts and non-Gaussian structure are never seen in the dynamic spectra of L bursts. The L burst modulation envelope is a manifestation of scintillation arising during propagation through the interplanetary medium, the original bursts having been of much longer duration when they left Jupiter's magnetosphere [*Douglas and Smith*, 1967].

Most of the powerful Jovian decametric noise storms observed between 15 and 27 MHz occur within two ranges of Central Meridian Longitude (CML), designated the Source B and Source A ranges. This longitude dependence is attributed to emissions from a common source region located in the north magnetic polar zone that are confined to hollow-cone beams having fixed opening half-angles of about 70° and cone axes that are tangent to the Jovian magnetic field at the emission points within the region. Radiation from each point is emitted at a frequency approximately equal to the local electron cyclotron frequency f_c. Whether the radiation is designated as Source B or Source A depends on which side of the hollow cone beams are aligned with Earth [*Dulk*, 1965]. The probability and intensity of such a storm are greatly enhanced if the magnetic flux tube passing through the Jovian moon Io also passes through

Copyright 1999 by the American Geophysical Union.

Paper number 1999JA900342.
0148-0227/99/1999JA900342$09.00

the above-mentioned north polar source region [*Bigg*, 1966]. There are thus Io-related and Io-independent Source B and A storms, designated Io-B, non-Io-B, Io-A, and non-Io-A. Io-B storms are of the highest occurrence probability and intensity, while non-Io-B are generally extremely weak. The occurrence of Source-A storms, particularly of non-Io-A, is strongly controlled by the Jovicentric declination of Earth, D_E [*Carr et al.*, 1970]. The sources of A and B emissions are located above the northern auroral zone, and the emissions are *X*-mode, right-hand elliptically or circularly polarized (in the frequency range in which we are interested). A third source region, designated C, is generally believed to be located above the southern auroral zone because its radiation is usually (but not always) polarized in the left hand sense. Its CML range immediately follows that of Source A, and its intensity-enhanced Io-C component occurs at the same Io configuration as that for Io-A. A review of the phenomenology of Jupiter's decametric radiation is given by *Carr et al.* [1983].

A second and less common type of Jovian decametric burst is the S burst, which occurs only in Io-related storms. The S and L in the burst-type designation stand for short and long, respectively [*Gallet*, 1961]. Unlike the L burst, the S burst possesses sharply defined dynamic spectral structure. Typical S bursts are quasi-repetitive, recurring at rates between about 2 and 400 s^{-1} over intervals of a few seconds, the most probable rate being about 20 s^{-1}. Each individual burst in such a series usually exhibits a negative frequency drift rate that is most often approximately -20 MHz s^{-1} (in the 15 to 27 MHz frequency range). The earliest papers on single-frequency observations of S bursts (made during the Jovian apparitions of 1956 and 1957) are those by *Kraus* [1956, 1958], *Carr et al.* [1958], and *Gallet* [1961]. The first dynamic spectral measurements of the distinguishing downward frequency drift rate of S bursts were made by *Warwick and Gordon* [1965] and *Riihimaa* [1966]. Other authors' papers or theses that have contributed to our knowledge of S bursts are *Baart et al.*, [1966], *Olsson and Smith* [1966], *Flagg and Carr* [1967], *Barrow and Baart* [1967], *Gordon and Warwick* [1967], *Paul* [1969], *Torgersen* [1969], *Goldreich and Lynden-Bell* [1969], *Riihimaa et al.* [1970], *Trapp* [1971], *Ellis* [1965, 1974, 1979, 1980, 1982], *Krausche et al.* [1976], *Kawamura and Suzuki* [1976], *Lynch et al.* [1976], *Riihimaa* [1977, 1979, 1991], *Desch et al.* [1978], *Flagg and Desch* [1979], *Leblanc et al.* [1980a, b], *Leblanc and Genova* [1981], *Riihimaa and Carr* [1981], *Staelin and Rosenkranz* [1982], *Alexander and Desch* [1984], *Zaitsev et al.* [1986], *Genova and Calvert* [1988], *Calvert et al.*, [1988], *Boev and Lukyanov* [1991], *Dulk et al.* [1992], *Ryabov* [1994], *Boudjada et al.* [1996], *Zarka et al.* [1996], and *Carr et al.* [1997].

For the purpose of this paper we define two types of S bursts, as follows:

1. Simple S bursts: The millisecond-scale dynamic spectrum of a group of simple S bursts, in which intensity is represented on a gray scale, appears as a set of sloping thin straight lines, all with nearly the same negative frequency drift rate. These drift rates differ for different storms but are nearly always between 15 and 30 MHz s^{-1}. The constant-time half-power bandwidth of each simple S burst in a millisecond-scale dynamic spectrum is in the vicinity of 10 kHz. An example of such a dynamic spectrum of a series of several simple S bursts is shown in Figure 1a.

2. Complex S bursts: The millisecond-scale dynamic spectra of the various subtypes of complex S bursts still possess components with consistently negative frequency drift rates but are more complicated than in the case of simple S bursts. The instantaneous bandwidths of complex S bursts are considerably greater than those of simple S bursts. Illustrations of a wide variety of complex S bursts, as well as of the much more rare simple S bursts, are given by *Flagg et al.* [1991].

About a decade after the discovery of Jupiter's decametric radiation by *Burke and Franklin* [1955], when radio observations from spacecraft at frequencies too low to penetrate the terrestrial ionosphere had become possible, Earth's auroral kilometric radiation (AKR) was first observed [*Benediktov et al.*, 1965]. *Wu and Lee* [1979] proposed the cyclotron maser instability (CMI) as the mechanism for the emission of AKR. This instability involves the direct amplification of electromagnetic fluctuations having frequency components near f_c by a stream of slightly relativistic electrons. The CMI model for AKR emission has gained widespread acceptance as the result of subsequent observational and theoretical work. However, a number of the problems concerning the model remain to be solved before we can have a good understanding of the emission process of AKR [*Pritchett and Winglee*, 1989].

It has generally been assumed, but not yet proven, that the CMI mechanism is also responsible for the emission of Jupiter's decametric, hectometric and kilometric radiation components and the hectometric, and kilometric components from Saturn, Uranus, and Neptune. Evidence for this is tentative, being based only on some degree of similarity of the outer-planet radio emissions to the AKR. In this paper we not only present detailed high-sensitivity measurements of the microstructure of the simplest possible Jovian decametric S bursts, but also demonstrate that these results tend to support the assumption that the cyclotron maser instability of *Wu and Lee* [1979] is the mechanism for the emission of Jovian S bursts.

2. Measurements

2.1. Instrumentation

The first published measurements of submillisecond structure within Jovian S bursts were made by *Flagg and Carr* [1967]. They obtained oscillographic intensity versus time photographs, with 10 μs resolution, of the intermediate frequency (IF) receiver output during Jo-

vian S burst storms that occurred at a frequency in the vicinity of 22.4 MHz. Highly significant structure was revealed down to the time resolution limit. Later, *Trapp* [1971], in his thesis research at the University of Florida, developed and made extensive use of an entirely analog tape-slowdown method for completely resolving plots of Jovian S burst voltage versus time from a receiver baseband output. By employing three successive stages of slowed-down tape playback, he was able to achieve an overall slowdown ratio of 8192 to 1, providing a time resolution of about 3 μs. Trapp verified the existence of the S burst fine structure reported by Flagg and Carr and obtained considerable information concerning the morphology of complex S bursts as received with an antenna of very low gain. These results differ somewhat from ours in the present paper, which were obtained from simple S bursts with an antenna of very high gain. Unfortunately, Trapp's results have appeared only in his unpublished thesis. We intend to present some of these results in a sequel to the present paper. Trapp's most important findings were that the complex S burst consists of a series of usually discrete pulses, most of which are of durations between 10 and 50 μs, as can be seen from Figure 5b, and that these pulses are individually frequency modulated. Their frequency drift rates can be either positive and negative, with magnitudes that are 2 orders of magnitude higher than that of the approximately –20 MHz s^{-1} drift rate that characterizes the S burst as a whole. As will be seen in the present paper, such enormously high-frequency drift rates do not generally occur in the microstructure of simple S bursts. We employ the term microstructure to indicate structural features in plots of intensity versus time and frequency (or of intensity versus time alone, as in the Flagg and Carr and Trapp measurements) obtained with a time resolution less than, say, 30 μs.

In the years following the early work of *Trapp* [1971], procedures were developed and extensively utilized for compiling catalogs of the full dynamic spectra of Jovian S bursts (i.e., intensity versus time and frequency). The inclusion of frequency information, however, was made at the expense of time resolution. The resolution limits of structure attainable in these dynamic spectra were about 0.3 ms in time and 3 kHz in frequency, hence our use of the term millisecond-scale structure as opposed to microstructure. The first extensive catalog of such dynamic spectra was that by *Ellis* [1979] at the University of Tasmania. The second was that by *Flagg et al.* [1991] of our University of Florida group. More recently, S burst dynamic spectra have been published by other groups, but none have sufficient time resolution to reveal the entirely different level of structural hierarchy with which this paper deals.

The simple S burst data analyzed here were obtained with the highly sensitive 640 dipole antenna array at the University of Florida Radio Observatory. This antenna has a half-voltage bandwidth of about 2 MHz, with a midfrequency of 26.3 MHz. For most of the measurements presented in this paper it was used in conjunction with a baseband receiver having a half-voltage bandwidth of about 280 kHz. The receiver converts the desired radio frequency (RF) band to baseband by subtracting the constant 25,950 kHz from each RF component. Thus the preconversion band of frequencies from 26,160 to 26,440 kHz becomes the baseband, spanning the frequencies from 210 to 490 kHz. The envelope of the frequency components remains essentially unchanged after the downconversion, and there is no appreciable loss of information regarding S burst structure on timescales greater than about 5 μs, which is the postdetector smoothing time we used in subsequent data analysis. The baseband receiver output is analog tape-recorded at a tape speed of 120 inches s^{-1} (304.8 cm s^{-1}). The tape is later played back at 1/128 times the recording speed, so that the frequency band now extends from 1641 to 3828 Hz. It is then passed into an audio spectrum analyzer, the output of which (in our original system) is displayed oscillographically as a spot exhibiting a brightness indicating intensity and a lateral deflection indicating frequency. In the measurement of dynamic spectra for our S burst catalog [*Flagg et al.*, 1991], the spot was photographed on film strip moving continuously in a direction perpendicular to the spot deflections, thus providing the dynamic spectrum. An example of the result is shown in Figure 1a, in which four of the simplest type of S bursts are seen.

In order to obtain a much finer time resolution and at the same time a somewhat better frequency resolution, we have replaced the analog spectrum analyzer at the receiver output by an analog-to-digital converter feeding into the memory of a computer (PC). The rate of sampling of the slowed-down data is 25,000 samples s^{-1}. This is equivalent to sampling the receiver output voltage directly (without the tape slowdown stage) at the rate 128 × 25,000, or 3.2×10^6, samples s^{-1}. The corresponding equivalent time between successive samples is 0.3125 μs. The simple S bursts that we selected for a preliminary analysis had band-limited durations of about 13 ms, most of them beginning or ending well outside our relatively narrow receiver passband. After verifying that the majority of these simple S bursts possessed similar microstructure, we selected a typical one for the detailed analysis that follows.

2.2. Subpulses

The simple S burst selected for an extensive microstructure analysis is indicated in Figure 1a. It was one of many similar bursts observed at 26.3 MHz during a late Io-A storm (277° CML; 235° Io phase; 222° Sub-Io Longitude) on Nov. 12, 1977, close to 0801:13 UT. The average frequency drift rate for the bursts in the storm was –19.5 MHz s^{-1}. The slow-playback output from the tape was digitized relatively recently. The timescale that we employ throughout this paper is the equivalent real-time scale (for both the baseband oscil-

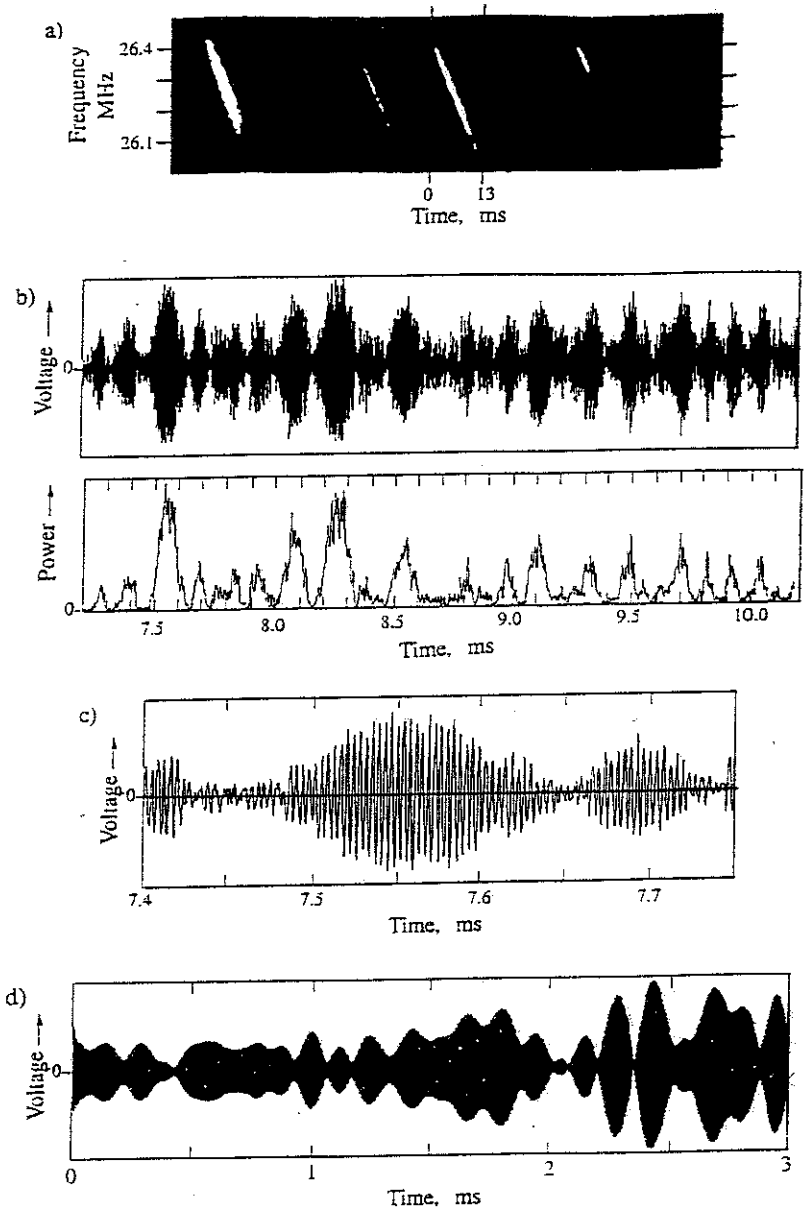

Figure 1. The simple S burst from the Io-A storm of November 12, 1977, that was selected for analysis. (a) Millisecond-scale dynamic spectrum. The burst that was analyzed is the third from the left. (b) (top) Oscillating voltage at the receiver baseband output plotted versus time for a 3 ms segment of the S burst. (bottom) Smoothed power (intensity) versus time for the same signal. (c) Section of the oscillating baseband voltage from Figure 1b, plotted on a fine enough timescale to resolve the individual oscillations. (d) Simulated subpulses in a narrow band (10 kHz bandwidth) of downward drifting quasi-sinusoidal frequency components having randomly selected phase constants; to be compared with Figure 1b.

lations and the corresponding preconversion RF oscillations) rather than that of the slowed-down tape playback. In Figure 1b (top), the receiver baseband output voltage is plotted versus time over a 3 ms segment of the 13 ms S burst of Figure 1a. Figure 1b (bottom) shows the result of passing this signal through a square-law detector in order to obtain the instantaneous power and then smoothing with a low-pass filter having a time constant of about twice the reciprocal of the baseband frequency (i.e., $\sim 5\ \mu s$). It is clear from this smoothed-power curve that the simple S burst is made up of a series of consecutive well separated pulses, generally of somewhat different maximum amplitudes and durations. This was also true of each of the other simple S bursts that we examined. We designate these pulses as subpulses.

In Figure 1b (top) the baseband oscillations (of ~350 kHz frequency) are obviously unresolved. Figure 1c shows the baseband voltage oscillation of two of the same subpulses on a sufficiently fine timescale that the

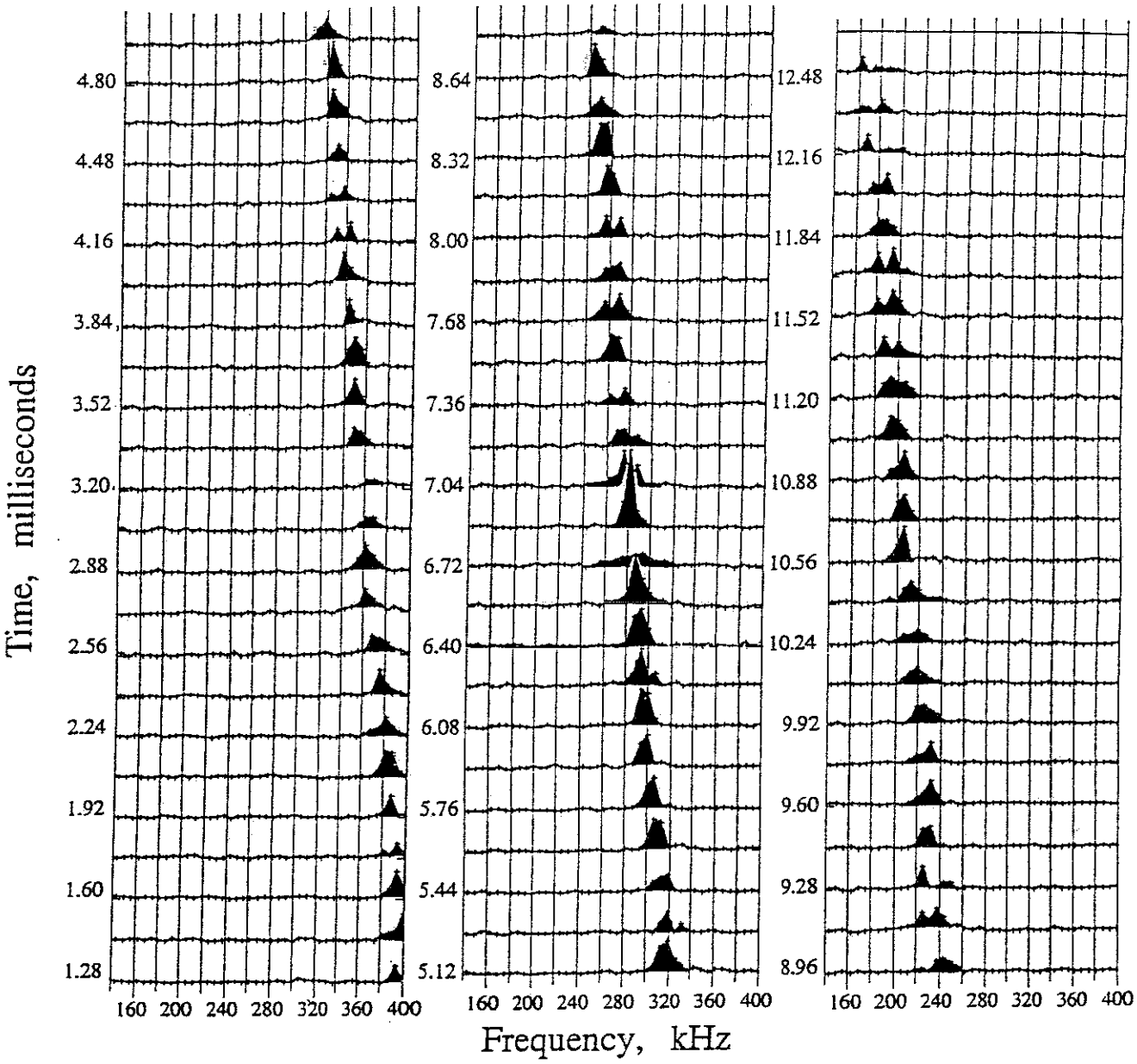

Figure 2. Plots of the magnitude of the Fourier transform as a function of baseband frequency, obtained from successive 0.16 ms intervals of the digitized S burst voltage-versus-time data. The frequency uncertainty corresponding to the 0.16 ms time uncertainty is 1/0.16 ms, or 0.62 kHz. The unusually high peak of the plot for the time value 6.88 ms (frequency 280 kHz) should be noted.

individual oscillation cycles beneath the envelope are resolved, making possible the approximate measurement of instantaneous frequency as a function of time. If we were able to display the corresponding oscillating RF voltage at the receiver input for the same time interval as in the top panel of Figure 1b, the result would be of similar appearance provided the same bandwidth had been employed. In this case the RF oscillations (frequency about 26,300 kHz) would of course also be unresolved, but the RF modulation envelope would be about the same as that of the baseband oscillation displayed in Figure 1b. The square-law-detected and smoothed RF version would also be very similar to the baseband version in the bottom panel of Figure 1b. Figure 1d, which should be compared with Figure 1b, shows a 3 ms segment of simulated subpulses obtained by summing a 10 kHz band of downward drifting quasi-sinusoidal frequency components having randomly selected phase constants. It will be discussed in section 3.2.

2.3. Application of the Fourier Transform

We obtained a dynamic spectrum of the simple S burst under investigation by means of repeated application of the fast Fourier transform (FFT) to the digi-

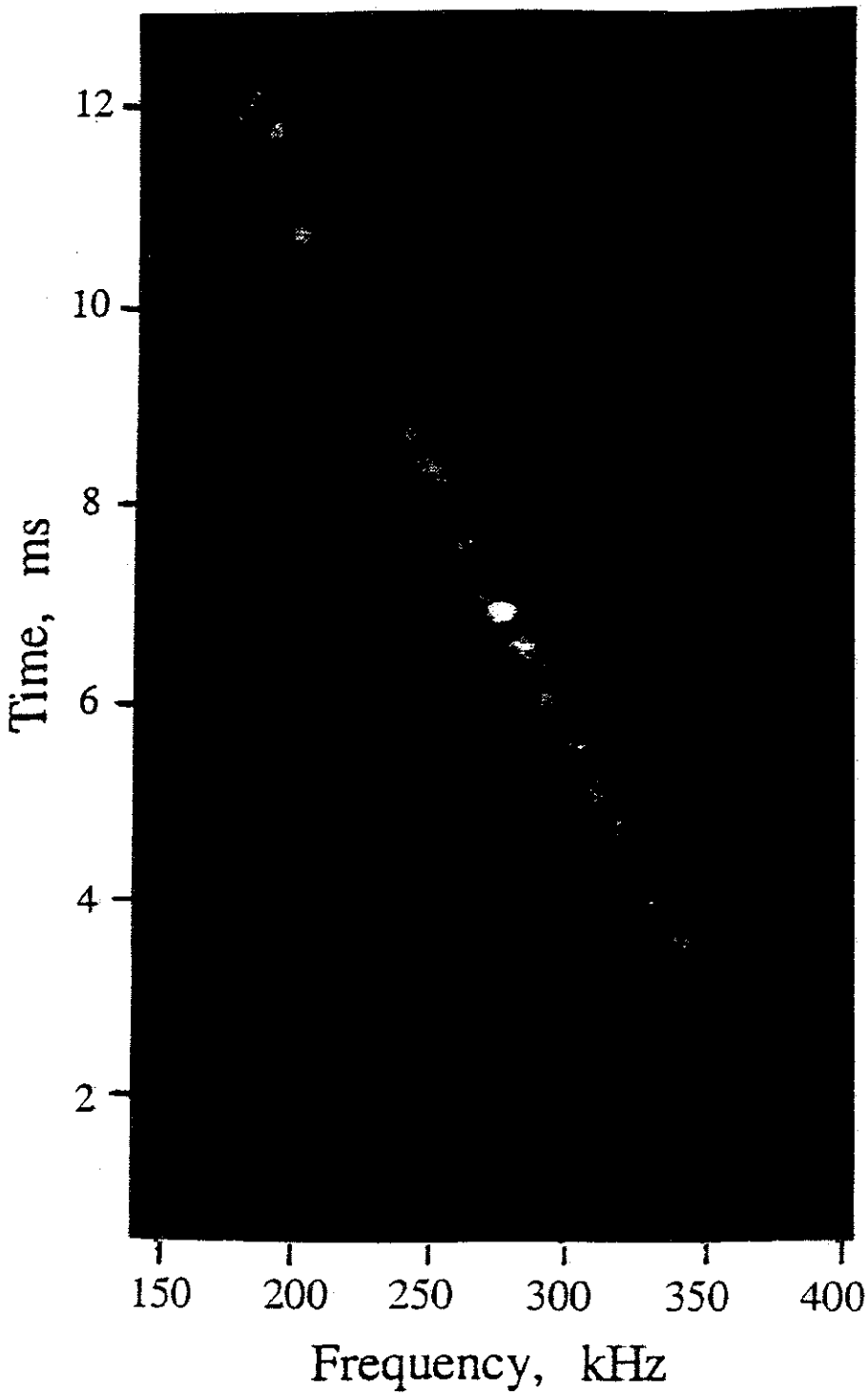

Figure 3. Gray-scale dynamic spectrum of the simple S burst obtained from the series of Fourier transform plots displayed in Figure 2. The bright spot centered on 6.88 ms is the unresolved image of the dominant subpulse pair, which is shown in Figure 4.

tized data of S burst voltage versus time. The complex FFT was calculated for each successive 0.16 ms data segment, and its magnitude (dimensions volts $Hz^{-0.5}$) was plotted as a function of baseband frequency. The result is shown in Figure 2. In order to estimate the mean frequency drift rate we plotted the frequency at the FFT magnitude peak versus the corresponding mid-time value for the successive 0.16 ms intervals, and fitted a straight line to the points. The frequency drift rate as determined by the slope of this line is -21.5 ± 1.2 MHz s^{-1}. Such negative frequency drifts of S bursts have long been attributed to gyroemission from clouds of electrons ascending the Io flux tube. Results from a model developed by *Zarka et al.* [1996] for S burst emit-

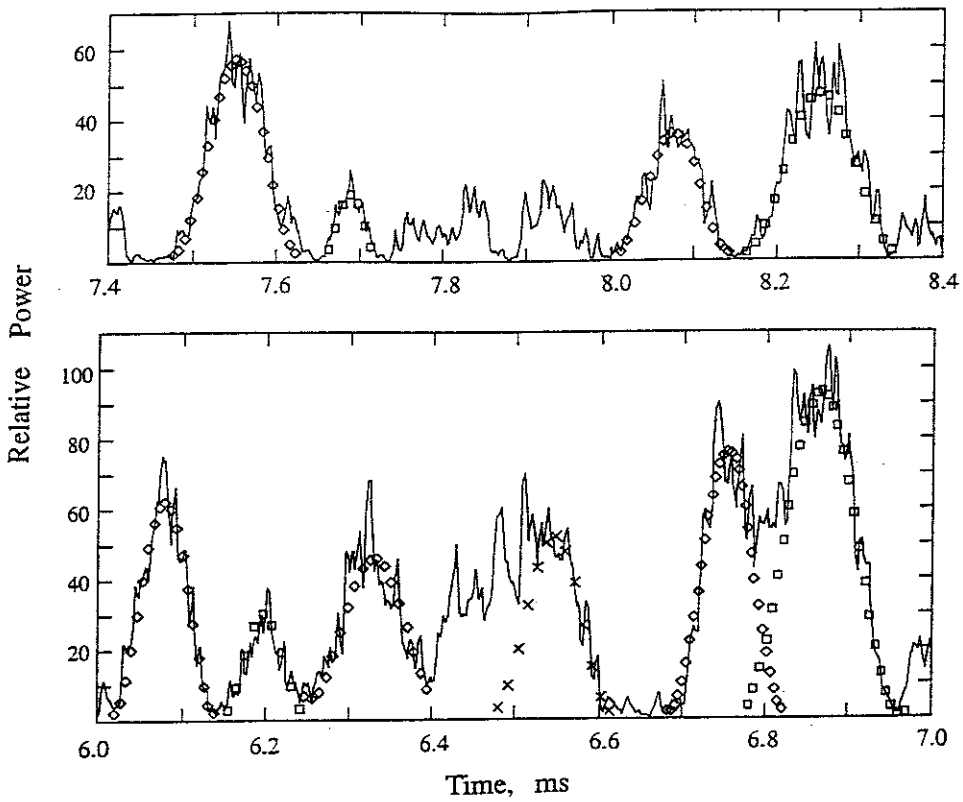

Figure 4. Power versus time plots of two sections of the simple S burst showing subpulses and the half-cycle cosine-squared fits to them (points of which are indicated by squares or diamonds). The overlapping pair of subpulses from 6.7 to 6.95 ms is unique in that the larger one is of maximum intensity and duration for the entire S burst, and unlike the other subpulses, they both exhibit phase coherence throughout their entire durations (as will be shown in Figure 6).

ting electrons trapped in an offset tilted dipole model of the Jovian magnetic field support this interpretation.

Figure 3 is a gray-scale plot of the same FFT data, the degree of whiteness being an indicator of the FFT magnitude at a given frequency and time. The gray scale has been adjusted so that only the more intense parts of the S burst are visible. The time and frequency resolution here are not fine enough that individual subpulses can consistently be identified. An outstanding feature of the plot in Figure 3 is the exceptionally bright spot centered on the time 6.88 ms (frequency = 280 kHz). A second outstanding feature is the distinct splitting into two components having slightly different slopes, near the end of the S burst. Such S burst splitting is common, as can be seen from the catalog of millisecond-scale S burst dynamic spectra by *Flagg et al.* [1991].

2.4. Characteristic Subpulse Waveform

We have found that most of the subpulse intensity (smoothed power) versus time plots are nearly symmetrical in shape except for some relatively weak superimposed structure and that the fundamental waveforms can be well fitted by half-cycle cosine-squared functions of adjustable widths and heights. The fitting function has the form

$$y = A\cos^2[\frac{\pi}{T}(t - t_0)] + y_0\,, \quad -\frac{T}{2} \le t_0 \le \frac{T}{2}\,. \qquad (1)$$

Here, t_0 is the time at the center of the subpulse, A and T are its height and width, and y_0 is the vertical offset, which is always very small. Figure 4 shows the results of such curve fitting for several of the larger subpulses. The two most intense subpulses for the entire S burst are the overlapping pair that occurred between 6.7 and 6.95 ms. We believe the irregular curve between 6.4 and 6.6 ms is the result of three or more overlapping subpulses, one of which we delineate by the "X" points. We presume that the irregular region between 7.73 and 8.0 ms is due to the overlapping of several weak and short subpulses. Reasonable fits with the cosine-squared function were obtained for a total of 48 subpulses within the single simple S burst. The histogram in Figure 5a indicates the distribution of their widths, in time. It should be noted that the most probable duration of these subpulses was about 90 μs and that none was less than 40 μs.

2.5. Highest-Resolution Measurements

We now make measurements of the S burst voltage oscillations $v(t)$, of which the subpulses are the envelope. These are the highest-resolution measurements of

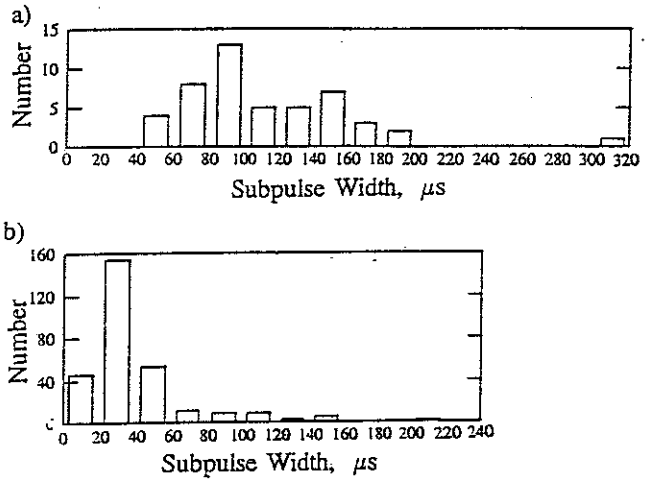

Figure 5. Distributions of subpulse durations: (a) for the simple S burst and (b) for several complex S bursts [from *Trapp* 1971].

S bursts from which significant information regarding their source can be obtained. Using the method described in section 2, we obtain digitized samples of baseband voltage versus time at a sampling period of 0.3125 μs. Any such quasi-sinusoidal voltage displaying a relatively slow frequency drift can be expressed equally well over a short time interval as either $\sin(2\pi f(t) + \delta_1)$ or $\sin(2\pi f_1 t + \delta(t))$, where δ_1 and f_1 are constants and the time variation is accounted for by either $f(t)$ or $\delta(t)$. We will usually employ the second type of expression and will refer to $\delta(t)$ as the variable phase term, in conjunction with a specified frequency.

We make use of a sinusoidal function generated in the computer, the frequency f_{lo} and phase constant δ_{lo} of which we can readily adjust. We refer to this function as the "local oscillator voltage". The monitoring of frequency (or phase) changes in $v(t)$ is made possible by successive comparisons with the local oscillator voltage. The procedure is as follows. A sequence of calculations is made of the cross correlation coefficient $C(f_{lo}, \delta_{lo})$ of $v(t)$ with $\cos(2\pi f_{lo} t + \delta_{lo})$ and of the coefficient $S(f_{lo}, \delta_{lo})$ of $v(t)$ with $\sin(2\pi f_{lo} t + \delta_{lo})$. Using these phase-quadrature correlations for a particular pair of values f_{lo} and δ_{lo}, successive calculations are made for plotting the function

$$\phi(t) = \arctan[\frac{S(t)}{C(t)}]. \qquad (2)$$

Successive averaging intervals of 3 μs are employed here. If we now express the S burst voltage as $v(t) = \sin(2\pi f_{lo} t + \delta(t))$, then $\phi(t) = \delta(t) - \delta_{lo}$. If values of f_{lo} and δ_{lo} can be found for which $\phi(t)$ is zero over some time interval, it follows that there is no measurable drift over the interval and that the frequency and phase constant of the local oscillator have been matched to those of the S burst.

In the search for a pair of values of f_{lo} and δ_{lo} that match the frequency and phase term of $v(t)$ over some time interval, the function $\phi(t)$ versus t is plotted for each pair of trial values. Generally, the curve drifts upward or downward with relatively smooth random changes in slope, but a value of f_{lo} can often be found for which some well-defined segment of the curve clearly remains constant. We will refer to it as a flat segment. Such flat segments are made conspicuous by their abrupt beginnings and endings (and are easily distinguished from situations in which the randomly drifting curve $\phi(t)$ may remain nearly constant as it smoothly passes through a maximum or minimum). Further adjustment of δ_{lo}, with slight readjustments of f_{lo}, will bring a flat segment approximately to zero, that is, will make $\phi(t) = 0$, the condition indicating the frequency and phase match over the segment.

Figure 6 illustrates results obtained from the application of this type of analysis to the overlapping pair of the most intense and longest lasting subpulses in the entire S burst. These two subpulses produced the brilliant spot centered on the time 6.88 ms in the dynamic spectrum of Figure 3. They are labeled A and B in the plot of relative smoothed power versus time in Figure 6a. Their region of overlap is labeled AB. Three overlapping sections of this plot are reproduced in Figure 6b for making time comparisons with corresponding curves in Figures 6c and 6d. In Figure 6c are three plots of the phase difference $\phi(t)$ versus t, time-aligned with the corresponding sections of the power versus t plot in Figure 6b. The pairs of vertical dotted lines in the three $\phi(t)$ plots delineate the flat segments mentioned above when the optimum values of f_{lo} and δ_{lo} are used in each case. The three values of optimum f_{lo} are listed under the heading "Baseband Frequency" in the table at the bottom, and the corresponding frequencies at the RF input of the receiver are also given. The three curves in Figure 6d are corresponding plots of the correlation coefficient of $v(t)$ with $\sin(2\pi f_{lo} t + \delta_{lo})$ when the optimum values of f_{lo} and δ_{lo} are employed. The correlation coefficient is 1.0 over each of the three flat segments, quickly falling to lower values on either side of the flat segment. It is clear that over each of the three contiguous time intervals A, AB, and B, the S burst oscillation was essentially phase coherent. The phase difference between the S burst oscillation and the monochromatic comparison signal never exceeded 12° over the three intervals between the pairs of dotted vertical lines. Furthermore, the onset and termination of the phase-coherent intervals were relatively abrupt. The frequencies at the RF input during the three intervals were 26.235 MHz for a duration of 61 μs, 26.231 MHz for a duration of 38 μs, and 26.229 MHz for a duration of 97 μs, respectively.

We suggest the possibility that within the S burst source a single powerful center of CMI wave amplification, emitting nearly monochromatic radiation, was active during intervals A and AB, and another even

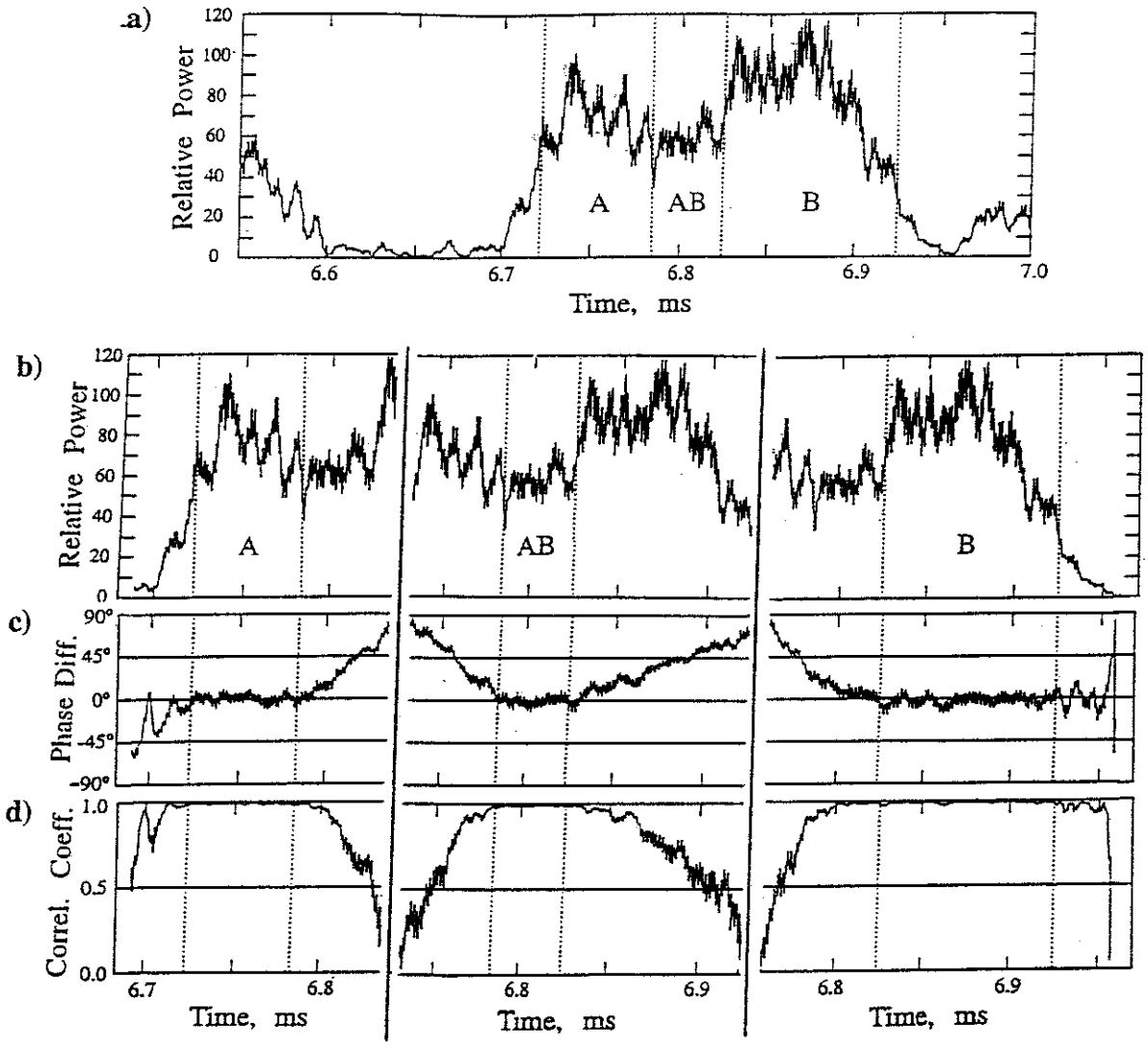

Section	A	AB	B
Baseband Freq.	285 kHz	281 kHz	279 kHz
RF Freq.	26.235 MHz	26.231 MHz	26.229 MHz
Duration	61 μs	38 μs	97 μs

Figure 6. The dominant subpulse pair within the simple S burst. (a) Power versus time plot. The two supersubpulses are indicated by A and B, and their region of overlap is AB. (b) The three sections of this panel are reproductions of parts of the power versus time plot of Figure 6a. (c) Each of the three sections is a plot of phase difference between the optimized (in-phase zero-beat) local oscillator signal and the S burst oscillation; the timescale of each one corresponds to that of the power versus time curve above it. The S burst baseband frequency in each case is given in the table, as is the corresponding input (preconversion) frequency. (d) Each of the three sections is a plot of correlation coefficient of the optimized local oscillator signal with that of the S burst oscillation at the baseband output. The pair of vertical dotted lines in each of the three sections of Figures 6b-6d indicate the beginning and ending times of the period of nearly zero phase difference and 1.0 correlation coefficient. The durations of these three intervals of coherence are given in the table.

more powerful one located slightly downstream from the first became active at a slightly lower frequency during interval AB and continued throughout B. Within the overlap period the resultant frequency was intermediate between those of A and B. These are the only two cases during the observable lifetime of the S burst, according to our interpretation, in which single powerful fixed-frequency cyclotron maser centers alone produced

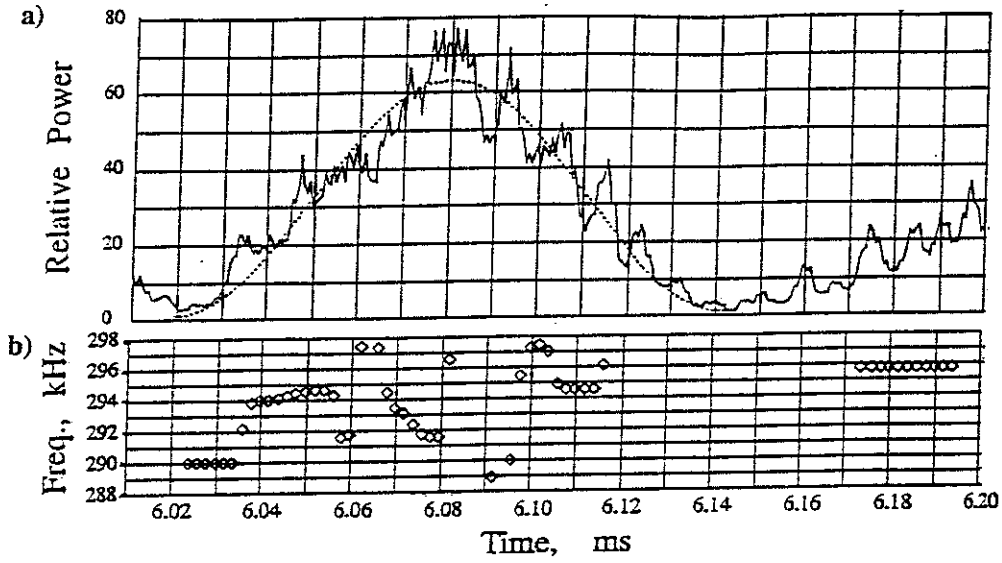

Figure 7. (a) Expanded-timescale plot of the subpulse centered on 6.08 ms. The dotted line is the cosine-squared half-cycle fit to the curve. (b) Successive values of the baseband frequency of the S burst as determined by local oscillator optimization. The gaps where points are missing indicate places at which the frequency was changing too erratically for a measurement to be made.

the entire subpulses in which they occurred (and the second of these subpulses was the longest and most intense in the entire S burst). In all other cases there were at most only a few relatively brief intervals of phase coherence within each subpulse, indicating that two or more maser centers contributed incoherently to the resultant radiation over most, but not all, of the duration of the subpulse. An example of the frequency variation within a more typical subpulse, showing how much of the time its radiation is incoherent and how much coherent, is presented in Figure 7.

The subpulse centered on the time value 6.08 ms in Figure 4 is reproduced with an expanded timescale in Figure 7a. The dotted line is the cosine-squared fit to the curve. The points representing individual measured frequency values are plotted in Figure 7b. The gaps in which there are no points are places at which the frequency was changing too erratically for a significant measurement to be made. In order for an interval to be phase-coherent the frequency over the interval must be constant. There are only two phase-coherent intervals in Figure 7b, the longest of which (of 20 μs duration) was actually within the weak subpulse following the one centered at 6.08 ms. We believe it was the confusion created by simultaneous emissions from multiple nearby centers of cyclotron maser activity that was responsible for the absence of phase coherence elsewhere in Figure 7.

3. Further Interpretation of Results

3.1. The Outward Moving Electron Stream

Ellis [1974] interpreted the characteristic downward frequency drift of S bursts, as observed on a millisecond timescale, to Doppler-shifted coherent cyclotron emission from recently mirrored adiabatically trapped electrons ascending the Io flux tube. According to this interpretation, the frequency decrease results from the motion of the electrons into a progressively weaker magnetic field. Several attempts have been made, first by Ellis and later by others, to match the motion of a recently mirrored adiabatically trapped electron to the observed decrease in S burst frequency with time. The earlier results were inconclusive. However, *Zarka et al.* [1996] demonstrated statistically, using large numbers of S bursts of diverse types, that a trapped electron model based on a modified offset tilted dipole (OTD) Jovian magnetic field model can be adjusted to yield frequency drift rates that are roughly consistent with those observed. For their S burst category most nearly resembling our simple nonforked Io-A type, they found the electron energy to be about 5 keV, approximately the same as the electron energy of the stream that drives the terrestrial cyclotron maser. The cyclotron maser, as it was first described to explain the terrestrial AKR [*Wu and Lee*, 1979] is located within a stream of electrons at a relatively short distance from a mirroring region in the geomagnetic field. In the original version of the cyclotron maser model, the pitch angle distribution of the recently mirrored electrons is deficient in those having pitch angles less than a certain value α_0, because of their collisional precipitation into the denser region (i.e., the upper ionosphere) before the points at which they would have mirrored were reached. Free energy associated with this loss cone distribution feeds the cyclotron maser instability at particular locations within the stream of mirrored electrons, resulting in the amplification of electromagnetic fluctuation frequency com-

ponents slightly higher than f_c. The emission beam of the amplified wave is a thin-walled hollow cone having a half-angle (opening in the outward direction) somewhat less than 85° with respect to the tangent to the magnetic field line. Io-B and Io-A S bursts are always polarized in the right-hand sense, and they no doubt originate in roughly the same region above the northern auroral zone. Their frequency drift is always downward because they are ascending the Io flux tube into ever weaker magnetic field intensity. The loss cone pitch angle distribution that supplies their power was established at their recent Northern Hemisphere mirroring. (Since this is a very unstable distribution, it could not last nearly long enough for the same electrons to emit another S burst with an upward frequency drift when they approached the southern auroral zone.) The left-hand polarized Io-C S bursts, which have the same sort of downward frequency drift as do the Io-B and Io-C ones, are probably emitted from electrons that have just mirrored in the Southern Hemisphere, at which time their required (but short-lived) loss cone distribution was established. It has been shown that other sources of free energy in addition to the loss cone distribution can drive the cyclotron maser instability that amplifies electromagnetic radiation.

In this section we demonstrate, using the O6 and VIP4 magnetic field models (rather than the OTD model employed by *Zarka et al.* [1996]) that the simple Io-A S bursts with which this paper is mainly concerned are compatible with the adiabatically trapped electron model. Our indicated electron energy is also in agreement with that generally accepted for the electrons that emit terrestrial AKR. To a first approximation, the magnetic fields of both Earth and Jupiter are dipolar, the dipole moment being offset somewhat from the center of the planet and tilted about 10° from the axis of rotation. An adiabatically trapped particle in such a field moves with constant kinetic energy and constant magnetic moment along a quasi-helical path enclosing a given tube of magnetic flux. If the particle is nonrelativistic and its radiation can be neglected, the magnitude v of its velocity vector $\mathbf{v}$ remains constant as the particle bounces back and forth between northern and southern mirror points. Only the direction of $\mathbf{v}$ changes with time. (We ignore the relativistic mass increase of the keV electrons with which we are concerned here, which is only 1% for a 5 keV electron, and the effect of radiation energy loss is very small outside regions of plasma instability.) Thus we assume that v = constant and $v_\perp^2/B$ = constant. For our selected simple Io-A S burst we use the following expression to calculate the electron velocity component parallel to B from the measured frequency drift rate df_c/dt:

$$v_\parallel = \frac{df_c/dt}{df_c/ds} \tag{3}$$

The value of df_c/dt for the selected typical simple Io-A S burst is -21.5 ± 1 MHz s^{-1}. The quantity df_c/ds is the gradient of f_c along the flux tube at the radio source. If the source were located in the same flux tube that is connected with Io (at a point where $f_c = 26.3$ MHz) at the time of emission of the S burst, the approximate source location and the value of df_c/ds could easily be determined from the magnetic field model together with the Sub-Io Longitude. However, there is an uncertain time interval, which is usually a delay, between the time Io and a given flux tube intersect and the time the resulting radio emission from that flux tube occurs. Since Jupiter's rotational angular velocity is considerably greater than Io's orbital angular velocity, the true West Longitude of the source may be somewhat different from that determined from the Sub-Io Longitude together with the field model if this unknown time lag is ignored. Such a time lag becomes a lead in the longitude of the radio source ahead of the Sub-Io Longitude (in addition to that which may be present owing to the inclination of field lines with respect to longitude meridians). A typical value of this anomalous lead angle increment is 30°. Because of the uncertainty in source longitude, it was necessary to examine the values of df_c/ds as determined from the O6 model over a wide longitude range bracketing possible source positions. It was found that for $f_c = 26.3$ MHz, df_c/ds was essentially constant over the entire Sub-Io Longitude range from 90° to 230°, its value being 1.19 ± 0.02 kHz km^{-1}. Inserting this gradient value and the measured frequency drift rate into (3), we obtain $v_\parallel = 18{,}000 \pm 1000$ km s^{-1} for the component of electron velocity parallel to B. The corresponding parallel-velocity kinetic energy is $1/2\, m v_\parallel^2 = 0.92$ keV.

A more restrictive lower limit on the total kinetic energy of an emitting electron can be determined by assuming for the moment that its mirror point was located at the foot of the Io-excited flux tube, at which point we represent f_c by f_{mir}. The total kinetic energy of the electron can then be found from

$$w = \frac{1}{2} m v_\parallel^2 \left[1 + \tan^2\left(\sin^{-1}\sqrt{26.3/f_{mir}}\right)\right]. \tag{4}$$

Since the mirror point of the actual electron could not have been located farther from the emission point than the flux tube foot, w as calculated from (4) can be considered to be a lower limit on the true electron energy. For the value of f_{mir} at the northern foot of the Io flux tube we first employ that given by the O6 model, which is 32.8 MHz. From (4) we find that the total energy of an electron that mirrored from such a location would be 4.6 keV. However, if the VIP4 field model of *Connerney et al.* [1998] is used instead, f_{mir} would be 43.6 MHz and the total energy would be 2.3 keV. Making the more conservative choice of these two values, we take 2.3 keV as the lower limit on the total energy of an average electron that was involved in the emission of our selected S burst.

We also made an upper limit estimate of the electron energy. To do this, however, it was necessary to select a simple Io-A S burst that was recorded from a receiver having a wider bandwidth. We will refer to it as burst 2

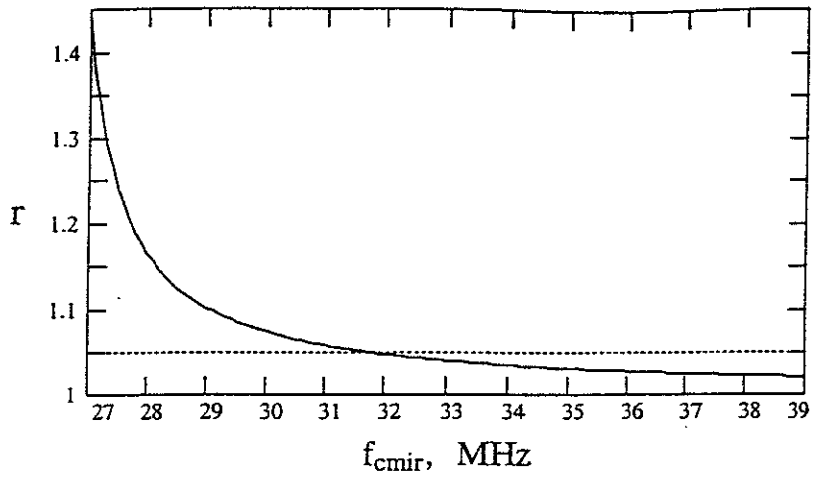

Figure 8. Plot of r (i.e., the ratio of the slopes of the midlines of the two halves of the S burst) versus f_{mir}, which is the electron cyclotron frequency at the point inside of which mirroring was unlikely for this value of r.

and the previous one as burst 1. Burst 2 was observed at a center frequency of 26.3 MHz with the Florida 640 dipole antenna array during an Io-A storm at 0144 UT on December 26, 1988. Its dynamic spectrum is displayed on page 150 of the S burst catalog of *Flagg et al.* [1991]. It is representative of those simple nonforked S bursts spanning the widest frequency range. The frequency drift rate, the parallel electron velocity component, and the lower-limit estimate of electron energy for burst 2 (based on the VIP4 field model) were found to be $df_c/dt = -29.3 \pm 0.4$ MHz s^{-1}, $v_{\|} = 24{,}600 \pm 500$ km s^{-1}, and $w > 4.3$ keV, respectively. The highest and lowest frequencies at which activity could be seen in the gray-scale image of the dynamic spectrum of burst 2 were 26.780 and 25.726 MHz, respectively. The median line along the image was examined under magnification for evidence of curvature. The line was divided into two equal segments, one centered at 26.517 MHz and the other at 25.990 MHz, and straight-line fits were made to the two segments. The frequency drift rate of the first segment was -29.0 ± 0.4 MHz s^{-1}, and that of the second was -29.7 ± 0.4. The ratio of the second to the first was $r = 1.02 \pm 0.03$, which is not significantly different from the value for a line without curvature. A value of r that is significantly > 1 would be consistent with a frequency drift rate that is becoming more negative as the electron gets farther from its mirror point, where the drift rate was momentarily zero. For an S burst observed at about 26.3 MHz, we have derived the following expression for the value of r as a function of the assumed cyclotron frequency value f_{mir} at the mirror point:

$$r = \sqrt{1 + \frac{f_{c1} - f_{c2}}{f_{mir} - f_{c1}}}, \qquad (5)$$

where f_{c1} and f_{c2} are the frequencies of the two segments, the values of which are given above. The ratio r as predicted by (5) is plotted versus f_{mir} in Figure 8. The horizontal dotted line represents $r = 1.5$, which is the upper boundary of the nominal uncertainty range of our measurement of r. At this r value, f_{mir} is 31.7 MHz, implying that the closest to the emission region that mirroring could have occurred without causing the S burst to display a measurable amount of curvature is the point at which $f_c = 31.7$ MHz. Insertion of this value into (4) and converting to electron volts yields 10.1 keV for the upper limit of the energy estimate based on burst 2.

To summarize the Io-A simple S burst source electron energy measurements, we find that the energy (per electron) in the case of burst 2 is $w = 7 \pm 3$ keV, and the estimated lower limit for burst 1 is 2.3 keV. These measured values are consistent with the nominal value of 5 keV for the energies of the electrons that emit the terrestrial auroral kilometric radiation. They are also consistent with the aforementioned result from *Zarka et al.* [1996] obtained by a method in which a simplified magnetic field model is employed.

3.2. Modeling Subpulses and Phase Coherent Segments

In our attempts to find an explanation for the S burst subpulse structure we have considered possible types of empirical models which we will refer to as the narrowband fluctuation model and the pulse superposition model. In a narrowband fluctuation model the subpulse waveform is a consequence of the statistical fluctuation in the successive sums of the instantaneous amplitudes of the large number of closely spaced but randomly phased frequency components by means of which narrowband Gaussian noise can be synthesized. Our first attempt at such a simulation consisted of the summation of 100 sinusoidal fixed-frequency voltage components, to which were assigned randomly chosen phase

constants, at equally spaced frequencies from a lower band limit of 345 kHz to an upper band limit of 355 kHz. The bandwidth was 10 kHz. Although the result produced envelope fluctuations very similar to actual S burst subpulses, the simulation was unrealistic in that it contained nothing to account for the characteristic downward frequency drift of S bursts. So we modified it by causing each of the 100 frequency components to drift downward in frequency at the rate -21.5 kHz ms^{-1} (i.e., 21.5 MHz s^{-1}), which was the measured drift rate of the S burst being modeled. The result is plotted in Figure 1d. The strong similarity of the simulated envelope fluctuations to those of the actual S burst subpulse envelopes shown in Figure 1b remained, except that the downward frequency drifts of the components introduced the increase in the maximum amplitudes of the envelope excursions with time that is apparent in Figure 1b. Such an amplitude increase does not appear in actual S burst noise. While it is possible that the amplitude increase could be eliminated by a modification to the simulation, this type of model for the production of subpulses has a more serious deficiency. The resultant radiation can never display intervals of phase coherence because of the decreasing frequency of each of the components.

We have concluded that a model based on the superposition of groups of pulses from closely spaced but independent short-lived emission centers that are nearly monochromatic but differ slightly in frequency would be more realistic than the fluctuation model. We will call it the pulse superposition model. In the pulse superposition model, which we have not yet constructed, an attempt will be made to duplicate more directly the effect of the superposition of the discrete pulses emitted from a small but ever-changing group of short-lived centers of cyclotron maser wave amplification traveling outward along the IFT with the beam of 7 keV electrons. It will be assumed that each such emission center emits a single pulse having a fixed "carrier frequency" equal to the local value of f_c, that is modulated by a curve representing the buildup and decay of wave amplification by that cyclotron maser. We will represent the modulating curve by a half cycle of a cosine-squared function. Emissions from those centers within the traveling group that are active at a given time are at slightly different frequencies because they experience slightly different magnetic field strengths. Thus the mean frequency of the emitted bandwidth decreases with time as the activity moves outward along the Io flux tube, the rate of frequency decrease being equal to the observed drift rate of the actual S burst. A distribution of the durations of the half-cycle cosine-squared modulating curves (i.e., of the pulse widths) will be assumed, and their peak amplitudes will be assumed to be proportional to their durations. The number of these amplification centers that are active as a function of time will also be an adjustable parameter. The morphology of the simulated subpulses produced by the model will depend strongly on both the assumed pulse width distribution and the assumed time variation of the number of amplification centers that are active. It will be only during intervals when just one powerful amplification center is active, which are usually but not always very brief, that phase coherent segments of the type actually observed will occur. We plan to compare results from this model, using different values of the adjustable parameters, with actual S burst subpulses and phase-coherent intervals until reasonable matches are obtained. We believe that this approach has promise.

4. Conclusion

Two new phenomena have been revealed in our investigation of the microstructure of Jovian simple S bursts. They are subpulses and phase-coherent segments. They promise to become an important source of information regarding the nature and particularly the small-scale structure of the emission mechanism. Much can undoubtedly be learned from obtaining more data of the same type as ours and from extending the investigation to simple S bursts from other source regions and to other types of spectrally structured Jovian bursts. An important question that has received little discussion in recent years is what causes the marked difference in the characteristics of S bursts and L bursts despite the fact that they appear to be emitted from nearly the same auroral zone regions into similar hollow-cone beams. It is clear that the L burst fine structure does not contain either subpulses or phase-coherent segments and that L bursts show no evidence at all of the frequency drift that is characteristic of S bursts. Theoretical studies of the AKR have led to the conclusion that the loss cone distribution is not the only means by which free energy can be supplied to the cyclotron maser [*Pritchett and Winglee*, 1989]. We suggest that L burst emission also results from CMI wave amplification, but in this case the required free energy is obtained from some other source than the loss cone distribution. Whatever the free energy source for L burst emission may be, we suggest that it is present not only in the S burst emitting regions but also in surrounding regions. This relatively wide distribution could perhaps account for the L burst characteristics of much wider bandwidth, much longer durations and higher occurrence probability. The absence of the negative frequency drifts alone is good evidence that the free energy of L-burst-emitting cyclotron masers is not derived from loss cone pitch angle distributions within isolated beams of recently mirrored electrons. The fact that the details of the emission mechanism for simple S bursts are beginning to be uncovered before those for L bursts may provide a new stimulus to theoretical activity regarding the latter.

Acknowledgments. The authors extend their thanks to Wesley B. Greenman, Jorge Levy, and Richard S. Flagg for much of the instrumentation development and data acquisition that made this work possible, to the two referees

who made suggestions for the improvement of the paper, and to Kazumasa Imai and James M. DeBuizer for valuable assistance in its preparation. Past support of the University of Florida Radio Observatory by the National Science Foundation is acknowledged.

Janet G. Luhmann thanks both of the referees for their assistance in evaluating this paper.

References

Alexander, J.K., and M.D. Desch, Voyager observations of Jovian millisecond radio bursts, *J. Geophys. Res.*, *89*, 2689–2697, 1984.

Baart, E.E., C.H. Barrow, and R.T. Lee, Millisecond radio pulses from Jupiter, *Nature*, *211*, 808–810, 1966.

Barrow, C.H., and E.E. Baart, B and C Sources of Jovian Decametric Radiation, *Nature*, *213*, 165–166, 1967.

Benediktov, E.A., G.G. Getmansev, N.A. Mitjakov, V.O. Rapoport, J.A. Sazonov, and A.F. Tarasov, Intensity measurements of radiation at frequencies 725 and 1525 Kc, by means of the receiver on the satellite Electron 2, *Space Res.*, *6*, 110–114, 1969.

Bigg, E.K., Periodicities in Jupiter's decametric radiation, *Planet. Space Sci.*, *14*, 741–758, 1966.

Boev, A.G., and M. Yu. Lukyanov, Theory of the decameter S radio emission of Jupiter, *Sov. Astron., Engl. Transl.*, 35(4), 422–427, 1991.

Boudjada, M.Y., P.H.M. Galopeau, and H.O. Rucker, Jovian S bursts: A discussion on the S burst drift model, *Astron. Astrophys.*, *306*, L9–L12, 1996.

Burke, B.F., and K.L. Franklin, Observations of a variable radio source associated with the planet Jupiter, *J. Geophys. Res.*, *60*, 213–217, 1955.

Calvert, W., Y. Leblanc, and G.R.A. Ellis, Natural radio lasing at Jupiter, *Astrophys. J.*, *335*, 976–985, 1988.

Carr, T.D., A.G. Smith, R. Pepple, and C.H. Barrow, 18–megacycle observations of Jupiter in 1957, *Astrophys. J.*, *127*, 274–283, 1958.

Carr, T.D., A.G. Smith, F.F. Donivan, and H.I. Register, The twelve-year periodicities of the decametric radiation of Jupiter, *Radio Sci.*, *5*, 495–503, 1970.

Carr, T.D., M.D. Desch, and J.K. Alexander, Phenomenology of magnetospheric radio emissions, in *Physics of the Jovian Magnetosphere*, edited by A.J. Dessler, chap. 7, pp. 226–284, Cambridge Univ. Press, New York, 1983.

Carr, T.D., K. Imai, L. Wang, L. Garcia, F. Reyes, C.H. Higgins, and W.B. Greenman, Recent results by the University of Florida Group from low frequency radio observations of Jupiter and Neptune, in *Planetary Radio Emissions, IV*, edited by H.O. Rucker, S.J. Bauer, and A. Lecacheux, pp. 25-41, Austrian Acad. of Sci. Press, Vienna, 1997.

Connerney, J.E.P., M.H. Acuna, N.F. Ness, and T. Satoh, New models of Jupiter's magnetic field constrained by the Io flux tube footprint, *J. Geophys. Res.*, *103*, 11,929–11,939, 1998.

Desch, M.D., R.S. Flagg, and J. May, Jovian S burst observations at 32 MHz, *Nature*, *272*, 38–40, 1978.

Douglas, J.N., and H.J. Smith, Interplanetary scintillation in Jovian decametric radiation, *Astrophys. J.*, *148*, 885–903, 1967.

Dulk, G.A., Io-related radio emission from Jupiter, Ph.D. thesis, Univ. of Colo., Boulder, 1965.

Dulk, G.A., A. Lecacheux, and Y. Leblanc, The complete polarization state of a storm of millisecond bursts from Jupiter, *Astron. Astrophys.*, *253*, 292–306, 1992.

Ellis, G.R.A., The decametric radio emission of Jupiter, *Radio Sci.*, *69D*, 1513–1530, 1965.

Ellis, G.R.A., The Jupiter radio bursts, *Proc. Astron. Soc. Aust.*, *2*, 1–8, 1974.

Ellis, G.R.A., An atlas of selected spectra of the Jovian S bursts, Physics Dep., Univ. of Tasmania, Hobart, Tasmania, 1979.

Ellis, G.R.A., The source of Jupiter S bursts, *Nature*, *283*, 48–50, 1980.

Ellis, G.R.A., Observations of the Jupiter S bursts between 3.2 and 32 MHz, *Aust. J. Phys.*, *35*, 165–175, 1982.

Flagg, R.S., and T.D. Carr, Wide bandwidth observations of the decametric bursts from Jupiter, *Astrophys. Lett*, *1*, 47–53, 1967.

Flagg, R.S., and M.D. Desch, Simultaneous multifrequency observations of Jovian S bursts, *J. Geophys. Res.*, *84*, 4238–4244, 1979.

Flagg, R.S., W.B. Greenman, F. Reyes, and T.D. Carr, A catalog of high resolution Jovian decametric noise burst spectra, Dep. of Astron., Univ. of Fl., Gainesville, 1991.

Gallet, R.M., Radio observations of Jupiter II, in *Planets and Satellites*, edited by G.P. Kuiper, pp. 500–533, Univ. of Chicago Press, Chicago, Ill. 1961.

Genova, F., and W. Calvert, The source location of Jovian millisecond radio bursts with respect to Jupiter's magnetic field, *J. Geophys. Res.*, *93*, 979–986, 1988.

Goldreich, P., and D. Lynden-Bell, Io, a unipolar inductor, *Astrophys. J.*, *156*, 59–78, 1969.

Gordon, M.A., and J.W. Warwick, High time resolution studies of Jupiter's radio bursts, *Astrophys. J.*, *148*, 511–540, 1967.

Kawamura, K., and I. Suzuki, A model of Jovian short duration bursts, *Astrophys. Lett.*, *18*, 19–23, 1976.

Kraus, J.D., Some observations of the impulsive radio signals from Jupiter, *Astron. J.*, *61*, 182–183, 1956.

Kraus, J.D., Planetary and solar radio emissions at 11 meters wavelength, *Proc. IRE*, *46*, 266–274 , 1958.

Krausche, D.S., R.S. Flagg, G.R. Lebo, and A.G. Smith, High resolution spectral analysis of the Jovian decametric radiation, I, Burst morphology and drift rates, *Icarus*, *29*, 463–475, 1976.

Leblanc, Y., and F. Genova, The Jovian S bursts, *J. Geophys. Res.*, *86*, 8546-8560, 1981.

Leblanc, Y., F. Genova, and J. de la Noe, The Jovian S bursts, I, Occurrence with L bursts and frequency limit, *Astron. Astrophys.*, *86*, 342–348, 1980a.

Leblanc, Y., M.G. Aubier, C. Rosolen, F. Genova, and J. de la Noe, The Jovian S bursts, II, Frequency drift measurements at different frequencies through several storms, *Astron. Astrophys.*, *86*, 349–354, 1980b.

Lynch, M.A., T.D. Carr, and J. May, VLBI measurements of Jovian S bursts, *Astrophys. J.*, *207*, 325–328, 1976.

Olsson, C.N., and A.G. Smith, Decametric radio pulses from Jupiter: Characteristics, *Science*, *153*, 289–290, 1966.

Paul, M.P. Waveform and source size studies of Jupiter's decametric radiation, Ph.D. dissertation, Dep. of Phys. and Astron., Univ. of Fl., Gainesville, 1969.

Pritchett, P.L., and R.M. Winglee, Generation and propagation of kilometric radiation in the auroral plasma cavity, *J. Geophys. Res.*, *94*, 129–143, 1989.

Riihimaa, J.J., High-resolution spectral observations of decametric radio bursts from Jupiter, *Ann. Acad. Sci. Fenn., Ser. A6*, 1–46, 1966.

Riihimaa, J.J., S bursts in Jupiter's decametric radio spectra, *Astrophys. Space Sci.*, *51*, 363–383, 1977.

Riihimaa, J.J., Drift rates of Jupiter's S bursts, *Nature*, *279*, 783–785, 1979.

Riihimaa, J.J., Evolution of the spectral fine structure of Jupiter's decametric S-storms, *Earth Moon Planets*, *53*, 157–182, 1991.

Riihimaa, J.J., and T.D. Carr, Interactions of S- and L-bursts in Jupiter's decametric radio spectra, *Moon Planets*, *25*, 373–387, 1981.

Riihimaa, J.J., G.A. Dulk, and J.W. Warwick, Morphology of the fine structure in the dynamic spectra of Jupiter's decametric radiation, *Astrophys. J. Suppl. Ser. 19 (172)*, 175–192, 1970.

Ryabov, B.P., Jovian S emission: Model of radiation source, *J. Geophys. Res.*, *99*, 8441–8449, 1994.

Staelin, D.H., and P.W. Rosenkranz, Formation of Jovian decametric S bursts by modulated electron streams, *J. Geophys. Res.*, *87*, 10,401–10,406, 1982.

Torgersen, H., Structural differences in Jupiter's millisecond pulses, *Phys. Norv.*, *3*, 195–202, 1969.

Trapp, B., An analysis of the microsecond pulse structure in Jupiter's decametric radio emission, M.S. thesis, Dep. of Phys. and Astron., Univ. of Fl., Gainesville, 1971.

Warwick, J.W., Radiophysics of Jupiter, *Space Sci. Rev.*, *6*, 841–891, 1967.

Warwick, J.W., and M.A. Gordon, Frequency and polarization structure of Jupiter's decametric emission on a 10 millisecond scale, *Radio Sci.*, *69D*, 1537–1542, 1965.

Wu, C.S., and L.C. Lee, A theory of the terrestrial kilometric radiation, *Astrophys. J.*, *230*, 621–626, 1979.

Zaitsev, V.V., E.Y. Zlotnik, and V.E. Shaposhnikov, The origin of S bursts in Jupiter's decametric radio spectra, *Astron. Astrophys.*, *169*, 345–354, 1986.

Zarka, P., T. Farges, B.P. Ryabov, M. Abada-Simon, and L. Denis, A scenario for Jovian S bursts, *Geophys. Res. Lett.*, *23*, 125–128, 1996.

T. D. Carr and F. Reyes, Department of Astronomy, University of Florida, 211 Bryant Space Science Center, PO Box 112055, Gainesville, FL 32611-2055. (e-mail: carr@astro.ufl.edu; reyes@astro.ufl.edu)

(Received June 4, 1999; revised July 26, 1999; accepted August 1, 1999.)